MnO_2-Embedded-in-Mesoporous-Carbon-Wall Structure for Use as Electrochemical Capacitors

Xiaoping Dong, Weihua Shen, Jinlou Gu, Liangmin Xiong, Yufang Zhu, Hua Li, and Jianlin Shi*

State Key Laboratory of High Performance Ceramics and Superfine Microstructures, Shanghai Institute of Ceramics, Chinese Academy of Sciences,1295 DingXi Road, Shanghai 20005095, People's Republic of China

Received: November 21, 2005; In Final Form: January 13, 2006

We present an in situ reduction method to synthesize a novel structured MnO_2/mesoporous carbon (MnC) composite. MnO_2 nanoparticles have been synthesized and embedded into the mesoporous carbon wall of CMK-3 materials by the redox reaction between permanganate ions and carbons. Thermogravimetric analysis (TG), X-ray photoelectron spectrum (XPS), X-ray diffraction (XRD), nitrogen sorption, transmission electron microscopy (TEM), and cyclic voltammetry were employed to characterize these composite materials. The results show that different MnO_2 contents could be introduced into the pores of CMK-3 treated with different concentrations of potassium permanganate aqueous solution, while retaining the ordered mesostructure and larger surface area. Increasing the MnO_2 content did not result in a decrease in pore size from the data of nitrogen sorption isotherms, indicating that MnO_2 nanoparticles are embedded in the pore wall, as evidenced by TEM observation. We obtained a large specific capacitance over 200 F/g for the MnC composite and 600 F/g for the MnO_2, and these materials have high electrochemical stability and high reversibility.

1. Introduction

Electrochemical capacitors are novel charge-storage devices of high power energy density, which exhibit excellent reversibility and a long cycle life. In recent years, electrochemical capacitors have attracted much attention for their higher power density compared to batteries and higher energy density compared to common capacitors.[1,2] According to the mechanism of energy storage, the electrochemical capacitors are classified as electric double-layer capacitors (EDLC) and faradaic pseudocapacitors. The former stored energy by charge separation formed at the interface between the electrode and the electrolyte. In the latter, the energy is mainly stored by a fast and reversible faradaic redox reaction in the electrode surface formed with electroactive materials, such as metal oxides. Among these materials, amorphous hydrated ruthenium oxide is one of the most attractive candidates for the electrode of electrochemical capacitors,[3,4] which exhibits ideal pseudocapacitive behavior, remarkably high specific capacitance (over 700 F/g), and excellent reversibility. However, the main disadvantage of ruthenium oxide is the high cost which greatly limited its practical application. Therefore, some cheap metal oxides, such as NiO, Co_3O_4, and MnO_2, have become promising alternative candidates as the electrodes of pseudocapacitors.[5−8]

Manganese oxides are considered as hopeful materials of pseudocapacitors not only due to the low cost but also their greater environmental compatibility than other metal oxides.[9−11] Coprecipitation,[12] thermal decomposition,[13] and sol−gel processes[14] have been developed for preparing manganese oxide electrodes. The specific capacitance of manganese oxides in the literatures generally ranges between 150 and 250 F/g.[15] Prasad and Miura[16] reported a capacitance value over 400 F/g in amorphous EMD deposited on stainless steel and much higher capacitance values in MnO_2-based mixed oxides.[17] However, these are still far from the theoretical value, ca. 1000 F/g, calculated in an MnO_2 alkaline battery.[15] As only the surface is involved in the pseudocapacitive behavior of manganese oxides, therefore enhancing the surface area should be an effective method to improve the specific capacitance.

Another key for manganese oxide to be used as an electrode of an electrochemical capacitor is to obtain high enough electrical conductivity. One of the most common methods is the direct deposition of manganese oxides on a carbon host, such as active carbon or carbon nanotubes.[15,16] The addition of carbon may increase the active sites, enhance the electric conductivity, improve the homogeneity of electrochemical reaction, and reduce the ionic resistance of the metal oxide and, consequently, further increase both the power and energy densities of the electrode.[18] Active carbons used as electric double-layer capacitors have been widely studied.[19−22] Unfortunately, even if they have large surface area, the application in electric double-layer capacitors is limited due to their micropores, which are less easily wetted by electrolytes, such that a large part of the surface exposed may not be utilized for charge storage.[23] To overcome this disadvantage, ordered mesoporous carbons with uniform mesopore size have become popular as an alternative EDLC material.[24,25]

A few papers have reported the loading of nanoparticles into the pores of ordered mesoporous carbons for lithium batteries and capacitors.[26−29] The ultrasound-induced formation of MnO_2 nanoparticles inside the mesopores of CMK-3 would usually lead to the disappearance of mesopores and the formation of micropores between the nanoparticles, which would prevent the mass transfer and also the formation of a double layer required for high-performance electrochemical capacitors. Herein, we present a new and facile method to prepare a MnO_2/carbon composite (MnC) by the direct reaction between the oxidant ($KMnO_4$) and the reductant (mesoporous carbon). The amount

* Corresponding author. Tel.: +86-21-52412714. Fax: +86-21-52413122. E-mail: jlshi@sunm.shcnc.ac.cn.

10.1021/jp056754n CCC: $33.50
Published on Web 03/07/2006

of manganese can be controlled according to the reaction time and the concentration of $KMnO_4$ aqueous solution. A novel and special structure of MnO_2 embedded in the mesoporous carbon wall was developed after the reaction, while the highly ordered pore structure, together with the initial pore size and volume, is maintained. Such a specially structured composite shows high electrochemical capacitor performance.

2. Experimental Section

For the synthesis of CMK-3 type carbons, SBA-15 was employed as a hard template. The synthesis of the mesoporous carbons was performed according to the procedure reported elsewhere.[30] Samples with different manganese contents were prepared using $KMnO_4$ aqueous solution with concentrations of 0.005, 0.01, and 0.05 M. In a typical loading procedure, 0.2 g of CMK-3 was dispersed into 50 mL of aqueous solution of $KMnO_4$ (0.005 M), and the mixture was stirred for 5 min at room temperature. After being filtered, the manganese-containing CMK-3 sample was washed with distilled water and, then, dried in air at 393 K. These samples were referred to as 0.005MnC-5, 0.01MnC-5, and 0.05MnC-5, respectively.

The content of MnO_2 in the composites was estimated by means of thermogravimetric analysis (TG, Netzsch STA-449C). X-ray photoelectron spectroscopy (XPS) analysis was carried out on a Vacuum Generators Microlab 310-F spectrometer equipped with Mg K (1253.6 eV) operating at 200 W. Powder X-ray diffraction (XRD) patterns were recorded on a Rigaku D/MAX-2250V diffractometer using Cu Kα radiation (40 kV and 40 mA). The scanning rate was 0.6°/min and 8°/min for the low-angle and high-angle XRD measurements, respectively. Nitrogen adsorption and desorption isotherms at 77 K were measured on a Micromeritics Tristar 3000 system. Transmission electron microscopy (TEM) images were obtained on a JEOL 200CX electron microscope operated at 160 kV. To prepare the working electrode, the active materials and poly(tetrafluoroethylene) (95:5, w/w) were mixed in ethanol, and the resulting mixture was pressed on the nickel foam substrate. The electrode was tested by cyclic voltammetry in 2 M KCl aqueous solution using a three-electrode system. A platinum sheet and a saturated calomel electrode (SCE) were used as the counter electrode and the reference electrode, respectively.

3. Results and Discussion

The MnC samples with different manganese contents were prepared using $KMnO_4$ aqueous solution with concentrations of 0.005, 0.01, and 0.05 M in 5 min, denoted as 0.005MnC-5, 0.01MnC-5, and 0.05MnC-5, respectively. The loading amount of manganese oxides on the CMK-3 was estimated from the residue contents after calcining the composite materials in air (subtracting the K_2O content measuring by ICP analysis). The 0.05MnC-5 sample has the highest MnO_2 loading, up to 26 wt %, and 0.01MnC-5 and 0.005MnC-5 are 13 and 9.4 wt %, respectively.

The surface information of the MnCs sample was collected by X-ray photoelectron spectroscopy (XPS). Figure 1 focuses on the region where the signals of Mn $2p_{3/2}$ and Mn $2p_{1/2}$ are expected to appear. The Mn $2p_{3/2}$ peak is centered at 642 eV and the Mn $2p_{1/2}$ peak at 653.8 eV, with a spin-energy separation of 11.8 eV. These results are in accordance with the reported data of Mn $2p_{3/2}$ and Mn $2p_{1/2}$ in MnO_2.[31] Additionally, no clear Mn $2p_{3/2}$ signal of $KMnO_4$ at 647 eV could be observed, proving that the permanganate ions have been reduced to manganese dioxide by the carbon in CMK-3.

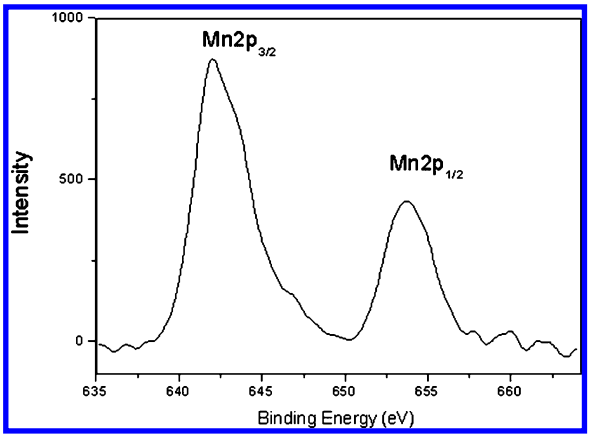

Figure 1. XPS spectra of the MnC sample for Mn $2p_{1/2}$ and Mn $2p_{3/2}$.

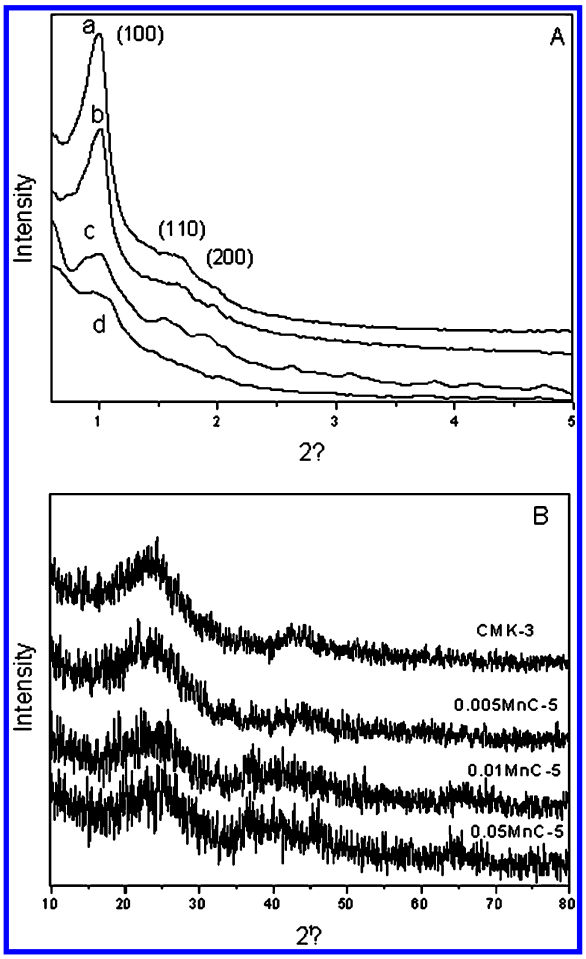

Figure 2. XRD patterns of CMK-3, 0.005MnC-5, 0.01 MnC-5, and 0.05 MnC-5 samples: (A) low-angle XRD patterns and (B) high-angle XRD patterns.

Figure 2A exhibits the low-angle X-ray diffraction (XRD) patterns of CMK-3 and MnO_2-loaded CMK-3 samples. The CMK-3 sample shows three well-resolved peaks that can be indexed as (100), (110), and (200) reflections associated with hexagonal symmetry. The three peaks can also be observed in 0.005MnC-5 and 0.01MnC-5 in the low-angle range; however, just only one peak of (100) was detected in the 0.05MnC-5 sample, which is mainly caused by the introduction of MnO_2 nanoparticles. There are no obvious MnO_2 diffraction peaks in the high-angle X-ray diffraction patterns of MnC samples compared to those of CMK-3 (Figure 2B), due to the amorphous nature of our reduced products.

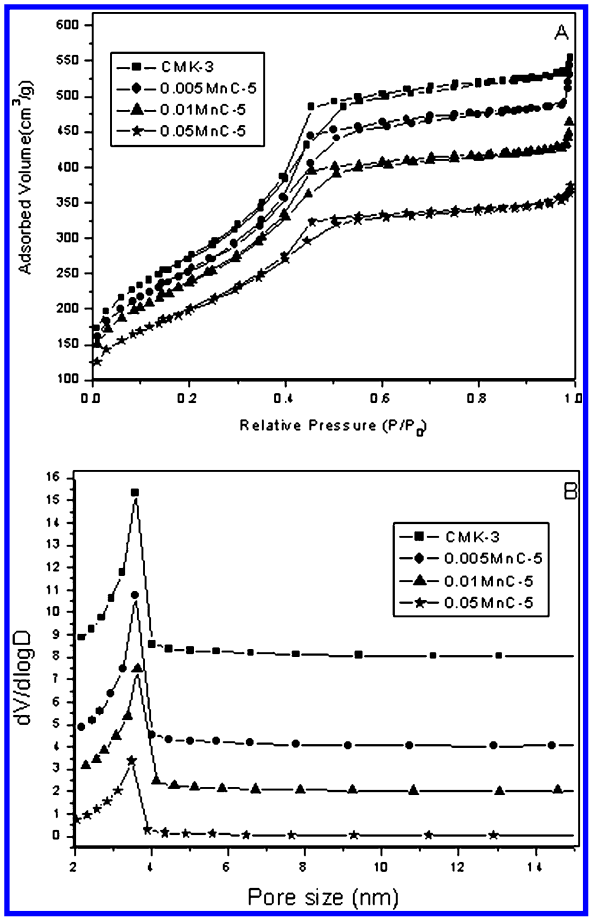

Figure 3. Nitrogen sorption isotherms (A) and the corresponding pore size distribution (B) for CMK-3, 0.005MnC-5, 0.01MnC-5, and 0.05MnC-5 samples, respectively.

TABLE 1: MnO_2 Contents and Pore Structure Parameters of the CMK-3 and MnC Samples

sample	CMK-3	0.005MnC-5	0.01MnC-5	0.05MnC-5
MnO_2 content (wt %)	0	9.4	13	26
surface area (m^2/g)	968	900	846	708
pore volume (cm^3/g)	0.96	0.94	0.82	0.57
pore size (nm)	3.6	3.6	3.6	3.5

Nitrogen sorption isotherms were recorded to access the pore properties of the samples. Figure 3A shows the nitrogen sorption isotherms of CMK-3, 0.005MnC-5, 0.01MnC-5, and 0.05MnC-5. All samples are found to be of type IV isotherm curves with a marked leap in the adsorption at relative pressures P/P_0 of 0.5, which is typical for mesoporous solids. This indicates that the ordered mesostructure of CMK-3 has been well kept. Large surface areas are retained after the insertion of MnO_2 nanoparticles, even at the MnO_2 content of 26 wt %. The surface area (Table 1) is found to decrease gradually from 968 m^2/g for CMK-3 to 900 m^2/g for 0.005MnC-5, 846 m^2/g for 0.01MnC-5, and 708 m^2/g for 0.05MnC-5. Similarly, the pore volume decreases also in this order, from 0.96 cm^3/g for CMK-3 to 0.57 cm^3/g for 0.05MnC-5. This decrease is, as we believe, mainly resulted from the higher density of MnO_2 than that of carbons rather than the pore-filling by MnO_2 as being confirmed by the data of average pore size (Table 1) and also the pore size distribution (Figure 3B). Pore-filling would significantly reduce the pore size,[32−34] even at relatively low loading level of guest materials; however, there is almost no reduction of pore size of our samples after the treatment with $KMnO_4$. Compared to the pore size of CMK-3, the greatest decrease is 0.1 nm for 0.05MnC-5, which possesses the highest MnO_2 content (26 wt %) in these samples. Therefore, according to the information from surface area, pore volume, and pore size, it is referred that most of MnO_2 nanoparticles do not exist in the mesopore channels.

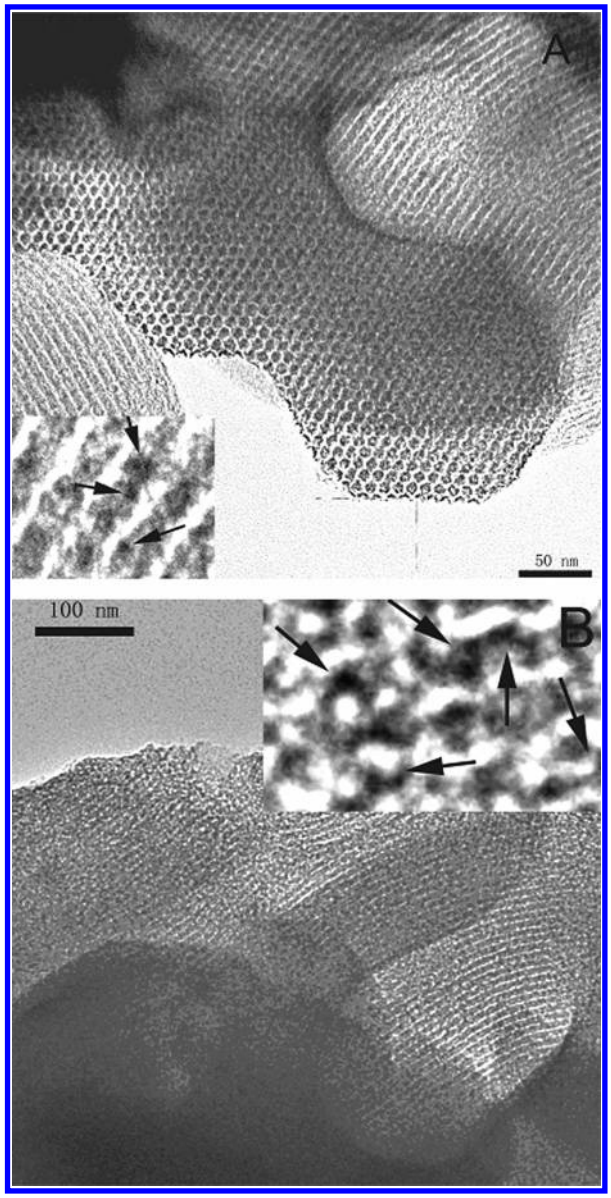

Figure 4. TEM images of (A) 0.005MnC-5 and (B) 0.05MnC-5 samples; the insets are the enlarged images.

Transmission electron microscopy (TEM) was used to directly observe the form of MnO_2 existing in the composite materials. Figure 4 reveals TEM photographs of 0.005MnC-5 and 0.05MnC-5. As the image shows, the ordered structure of CMK-3, an exactly negative replica of SBA-15 with a hexagonal arrangement of cylindrical mesoporous tubes, has been preserved after different amounts of manganese dioxides were loaded. The similar pore sizes, about 3.5−4 nm in the mesopore range, were observed in TEM images of 0.005MnC-5, 0.01MnC-5, and 0.05MnC-5, which are in accordance with the pore size distribution analysis from nitrogen sorptions. No bulk aggregates of MnO_2 can be found outside of the CMK-3 particles, and also no nanoparticles of larger size than the pore size of CMK-3 can be observed. In addition, the data of pore size and BET surface area suggest that most of MnO_2 nanoparticles do not exist in the pore channels. Therefore, the other possibility is that MnO_2 nanoparticles have been embedded in the wall of

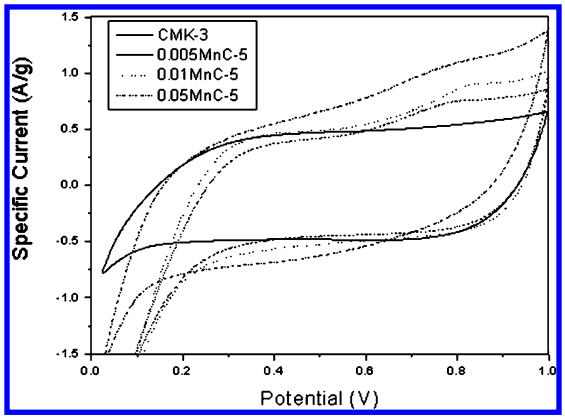

Figure 5. CV curves for CMK-3, 0.005MnC-5, 0.01MnC-5, and 0.05MnC-5 in 2 M KCl aqueous solution at 5 mV/s.

CMK-3. The TEM images of MnCs provide a direct evidence for this deduction. Obvious contrast within the wall can be identified; while no materials exist in pore channels, the dark area should be MnO_2 nanoparticles due to its much higher density than carbon, and this means that large amount of MnO_2 nanoparticles have been embedded into the wall, as shown in the insets.

Figure 5 shows the cyclic voltammograms (CVs) of CMK-3 and MnC composite electrodes with different manganese dioxide loading levels in 2 M KCl aqueous solution under a potential in the range from 0 to 1.0 V with a scan rate of 5 mV/s. The CVs are not nearly rectangles, which indicates that the ohmic resistance for electrolyte motion in the carbon pores has affected the double-layer formation mechanism. The induced current would intensify the potential difference between the mouth and the bottom of the pores and, thus, resulted in the delayed current response as shown in the tilted voltammograms. This nonideal behavior was also found in the capacitance of mesoporous carbon with the rate of 5mv/s in the literature (ref 24). Upon increasing the manganese dioxide content from 0 to 26 wt %, the specific current becomes larger gradually, which is the result of a contribution from the pseudocapacitive manganese dioxide component. The specific capacitance was calculated from the equation, $C = I/(\upsilon m)$, where I is the current in the cyclic voltammogram, υ is the scan rate, and m is the mass of the active materials. Within the range of weight percentage of manganese dioxides, 0−26 wt %, the specific capacitances increase nearly linearly and reach 220 F/g at 26 wt %. After subtracting the electric double-layer capacitance contributed by mesoporous carbon CMK-3, the manganese dioxide component exhibits very high capacitance. At relatively low manganese dioxide loading level, 9.4 and 13 wt %, the MnO_2-based capacitances are 605 and 628 F/g, respectively, over 60% of the theoretical value calculated from a MnO_2 alkaline battery. As we know, only the surface is involved in the pseudocapacitive behavior of manganese oxides. However, our new structure of MnO_2 embedded in the mesoporous carbon wall can provide both large MnO_2 surface area and good electric conductivity, which contributes for the enlarged electrochemical capacitance. The specific capacitance of the manganese dioxide component in the 0.05MnC-5 sample, 547 F/g, is a little smaller than those of samples with low manganese oxide loading, due to the bigger size of the manganese oxide nanoparticles at the high manganese oxide loading level. The relationship between the specific capacitance of the MnC composite and the scan rate is listed in Table 2. The slight capacitance decrease with the scan rate indicates that such a novel structure allows a rapid diffusion of ions.

TABLE 2: Specific Capacitance of CMK-3 and MnC Samples[a]

scan rate of CV	C_{MnC} (F/g)			C_{Mn} (F/g)		
	5 mV	20 mV	50 mV	5 mV	20 mV	50 mV
CMK-3	105	96	83			
0.005MnC-5	152	142	123	605	585	509
0.01MnC-5	173	155	130	628	550	445
0.05MnC-5	220	186	156	547	442	364

[a] Data of the specific capacitance of MnO_2 are calculated from the equation, $C_{Mn} = (C_{MnC} - C_C C\%)/Mn\%$, where C_{Mn}, C_{MnC}, and C_C are the specific capacitance of MnO_2, the MnC composite, and pure CMK-3 and C% and Mn% are the weight percentages of C and MnO_2 in the MnC composite, respectively.

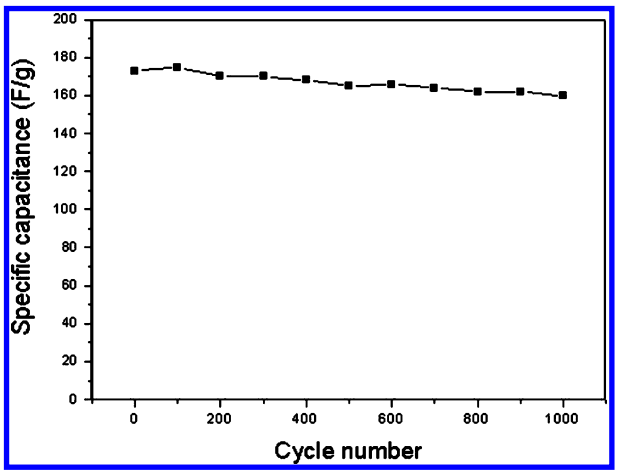

Figure 6. Specific capacitance of the 0.01MnC-5 electrode in 2 M KCl aqueous solution at 5 mV/s as a function of the cycle number.

The electrochemical stability of the active material and its repeatability were investigated by cyclic CV measurements. Figure 6 shows the relationship between cycle number and the capacitance of the 0.01MnC-5 sample. After 1000 cycle tests, the specific capacitance of 0.01MnC-5 decreased slightly from 173 F/g to 160 F/g, i.e., 92% of the original value was maintained. This result reveals that these active materials as pseudocapacitors have good pseudocapacitor properties with high electrochemical stability.

4. Conclusion

In summary, the novel structure of MnO_2 embedded in the mesoporous carbon wall has been synthesized by a new in situ reduction process. Permanganate ions in aqueous solution were reduced to manganese dioxides by the carbon atoms on the surface of CMK-3, and C−C bonds were oxidized. The MnO_2 nanoparticles were directly observed in the TEM image studded and embedded in the carbon walls and did not block the pore openings, which is important for the mass-transfer process in the electrode reaction. Consequently, a large specific capacitance of over 200 F/g for the MnC composite and 600 F/g for the MnO_2 were obtained, and these materials have high electrochemical stability and high reversibility.

Acknowledgment. This work was supported by the Natural Science Foundation of China (50232050), the National Fundament Research Project (2002CB613305), the National Hi-Tech Project (2002AA321010), the Shanghai Special Project (03DJ14004), and the Foundation of Shanghai Nanotechnology (0452nm056, 05nm05030).

References and Notes

(1) Conway, B. E. *J. Electrochem. Soc.* **1991**, *138*, 1539−1548.
(2) Arbizzani, C.; Mastragostino, M.; Soavi, F. *J. Power Sources* **2001**, *100*, 164−170.
(3) Zheng, J. P.; Cygan, P. J.; Jow, T. R. *J. Electrochem. Soc.* **1995**, *142*, 2699−2704.
(4) Zheng, J. P.; Jow, T. R. *J. Electrochem. Soc.* **1995**, *142*, L6−L8.
(5) Liu, K.-C.; Anderson, M. A. *J. Electrochem. Soc.* **1996**, *143*, 124−130.
(6) Nam, K. W.; Kim, K. B. *J. Electrochem. Soc.* **2002**, *149*, A346−A354.
(7) Kim, H. S.; Popov, B. N. *J. Electrochem. Soc.* **2003**, *150*, D56−D62.
(8) Kim, H. K.; Seong, T. Y.; Lim, J. H. *J. Power Sources* **2001**, *102*, 167−171.
(9) Lee, H. Y.; King, S. W.; Lee, H. Y. *Electrochem. Solid−State Lett.* **2001**, *4*, A19−A22.
(10) Jiang, J.; Kucernak, A. *Electrochim. Acta* **2002**, *47*, 2381−2386.
(11) Hu, C. C.; Tsou, T. W. *J. Power Sources* **2003**, *115*, 179−186.
(12) Lee, H. Y.; Goodenough, J. B. *J. Solid State Chem.* **1999**, *144*, 220−223.
(13) Lee, H. Y.; Manivannan, V.; Goodenough, J. B. *C. R. Chim.* **1999**, *2*, 565−577.
(14) Pang, S. C.; Anderson, M. A.; Chapman, T. W. *J. Electrochem. Soc.* **2000**, *147*, 444−450.
(15) Raymundo-Pinero, E.; Khomenko, V.; Frackowiak, E.; Beguin, F. *J. Electrochem. Soc.* **2005**, *152*, A229−A235.
(16) Prasad, J. R.; Miura, N. *J. Power Sources* **2004**, *135*, 354−360.
(17) Prasad, J. R.; Miura, N. *Electrochem. Commun.* **2004**, *6*, 1004−1008.
(18) Chang, J.-K.; Lin, C.-T.; Tsai, W.-T. *Electrochem. Commun.* **2004**, *6*, 666−671.
(19) Tanahashi, I.; Yoshida, A.; Nishino, A. *Carbon* **1990**, *28*, 477−482.
(20) Yoshida, A.; Tanahashi, I.; Nishino, A. *Carbon* **1990**, *28*, 611−615.
(21) Biniak, S.; Dzielendziak, B.; Siedlewski, J. *Carbon* **1995**, *33*, 1255−1263.
(22) Soneda, Y.; Toyoda, M.; Hashiya, K.; Yamashita, J.; Kodama, M.; Hatori, H.; Inagaki, M. *Carbon* **2003**, *41*, 2680−2682.
(23) Jang, J. H.; Han, S.; Hyeon, T.; Oh, E. M. *J. Power Sources* **2003**, *123*, 79−85.
(24) Liu, H.; Wang, K.; Teng, H. *Carbon* **2005**, *43*, 559−566.
(25) Alvarez, S.; Blanco-Lopez, M. C.; Miranda-Ordieres, J. A.; Fuertes, A. B.; Centeno, T. A. *Carbon* **2005**, *43*, 855−857.
(26) Zhu, S.; Zhou, H.; Hibino, M.; Honma, I.; Ichihara, M. *Adv. Funct. Mater.* **2005**, *15*, 381−386.
(27) Fan, J.; Wang, T.; Yu, C.; Tu, B.; Jiang, Z.; Zhao, D. *Adv. Mater.* **2004**, *16*, 1432−1436.
(28) Choi, W. C.; Woo, S. I.; Jeon, M. K.; Sohn, J. M.; Kim, M. R.; Jeon, H. J. *Adv. Mater.* **2005**, *17*, 446−451.
(29) Joo, S. H.; Choi, S. J.; Oh, I.; Kwak, J.; Liu, Z.; Terasaki, O.; Ryoo, R. *Nature* **2001**, *412*, 169−172.
(30) Fuertes, A. B.; Nevskaia, D. M. *Microporous Mesoporous Mater.* **2003**, *62*, 177−190.
(31) Tan, B. J.; Klabunde, K. J.; Sherwood, P. M. A. *J. Am. Chem. Soc.* **1991**, *113*, 855−861.
(32) Zhang, W.; Shi, J.; Chen, H.; Hua, Z.; Yan, D. *Chem. Mater.* **2001**, *13*, 648−654.
(33) Zhang, L.; Shi, J.; Yu, J.; Hua, Z.; Zhao, X.; Ruan, M. *Adv. Mater.* **2002**, *14*, 1510−1513.
(34) Li, L.; Shi, J.; Zhang, L.; Xiong, L.; Yan, J. *Adv. Mater.* **2004**, *16*, 1079−1082.